GEOLOGICAL SURVEY OF CANADA
OPEN FILE 6957

Determination of geothermal gradient from borehole temperature and permafrost base for exploration wells in the Beaufort-Mackenzie Basin

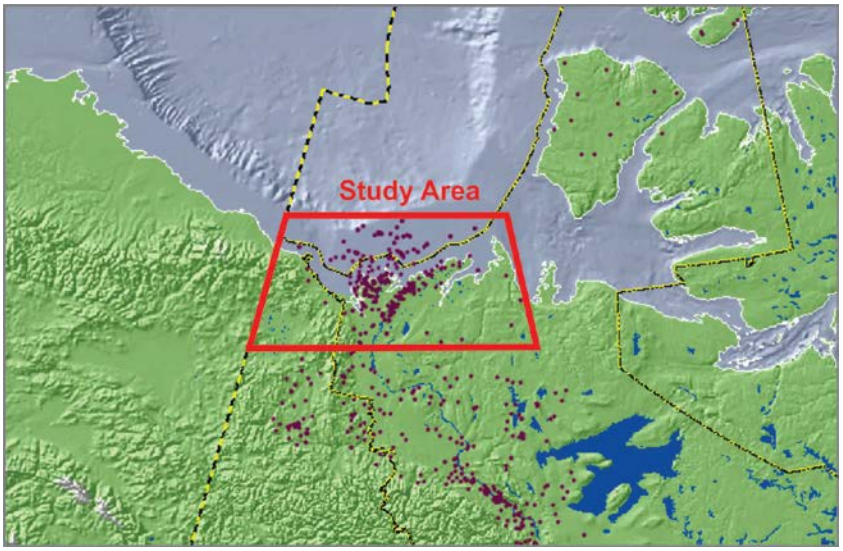

The original image was provided by T.A. Brent

K. Hu, Z. Chen, and D.R. Issler

2014

Natural Resources Canada | Ressources naturelles Canada

Canada

GEOLOGICAL SURVEY OF CANADA
OPEN FILE 6957

Determination of geothermal gradient from borehole temperature and permafrost base for exploration wells in the Beaufort-Mackenzie Basin

K. Hu, Z. Chen, and D.R. Issler

2014

doi:10.4095/293872

This publication is available for free download through GEOSCAN (http://geoscan.nrcan.gc.ca/).

Recommended citation:
Hu, K., Chen, Z., and Issler, D.R., 2014. Determination of geothermal gradient from borehole temperature and permafrost base for exploration wells in the Beaufort-Mackenzie Basin; Geological Survey of Canada, Open File 6957, 23 p. plus figures and table. doi:10.4095/293872

Publications in this series have not been edited; they are released as submitted by the author.

TABLE OF CONTENTS

SUMMARY

Geothermal gradient is a useful parameter for constraining models of heat flow and petroleum generation in sedimentary basins. This report documents geothermal gradient values for the exploration wells that were used to construct a geothermal gradient map for the Beaufort-Mackenzie Basin. First-order, linear geothermal gradients were calculated for 259 Beaufort-Mackenzie petroleum exploration wells using subsurface temperature data obtained during well testing and logging. Geothermal gradients were determined by applying a least-square fit to the deep temperature data with the requirement that they intersect the mapped base of permafrost at an assumed temperature of 0 ºC. Geothermal gradient values were quality-assessed based on the quality and quantity of the individual temperature points used for the calculations and the quality of the fit to the data as represented by the coefficient of determination. Results are displayed graphically as plots of temperature versus depth with respect to fitted linear geothermal gradients for specific well locations. Examples are used to illustrate some anomalous temperature data that have been excluded from the calculation of geothermal gradient. For example, anomalously low DST temperature values in gas zones can be attributed to the Joule-Thomson effect related to gas expansion caused by the pressure drop that accompanies flow. Calculated geothermal gradients vary from approximately 15 °C/km to 48 °C/km across the Beaufort-Mackenzie Basin, and a large fraction of the basin is characterized by typical sedimentary basin geothermal gradients of 25 °C/km to 35 °C/km (> 200 wells).

INTRODUCTION

Temperature is a fundamental parameter in the formation of petroleum and mineral deposits, and in the assessment of geothermal energy resources. Geothermal gradient is defined as the rate of change of temperature with depth in the earth. Maps of geothermal gradient are important for the petroleum and geothermal energy industries because they can be used to provide estimates of the subsurface temperature variation within sedimentary basins. Such information is relevant for calibrating basin thermal models for petroleum generation (e.g. Barker, 1996) and for delineating commercially exploitable geothermal energy reserves (e.g. Grasby *et al*., 2012).

Thermal data are sparse or absent over large parts of Canada (Grasby *et al*., 2012) although geothermal gradient maps are available for specific regions including the eastern (Issler, 1984; Moir and Bell, 1989) and arctic continental margins (Majorowicz *et al*., 1996; Majorowicz and Embry, 1998; Issler *et al*., 2011), and the western and northwestern interior basins (Majorowicz *et al*., 1988; Bachu and Burwash, 1994; Majorowicz and Morrow, 1998; Majorowicz *et al*., 2005). Early investigations of the deep thermal regime of the Beaufort-Mackenzie region (e.g. Jones *et al*., 1988; Majorowicz *et al*., 1988; Jones *et al*., 1990; Majorowicz *et al*., 1990) occurred during the first cycle of petroleum exploration (1962-1992) and culminated in the publication of a geothermal gradient map (Majorowicz *et al*., 1996) based on temperature data for 188 wells (representing wells drilled up to approximately 1985). In 2000, a second phase of exploration began and new geothermal studies were initiated to include data from wells drilled after the mid-1980s. More than 280 oil and gas exploration wells have been drilled in the Beaufort-Mackenzie Basin since 1965. Most of these wells have point-wise temperature data that were collected during logging and well testing operations. Hu *et al*. (2010) compiled and quality-assessed temperature data for 258 petroleum exploration wells drilled in the area between 1965 and 2007 as part of a larger government-industry funded study of petroleum systems of the Beaufort-Mackenzie region that was active during 2001-2013. The temperature data consist of log-based maximum bottomhole temperature (BHT) measurements (corrected for the cooling effects of mud circulation where possible) and maximum well fluid test temperatures (primarily from drillstem tests).

Chen *et al*. (2008) analysed the spatial variation in the well temperature data and suggested that many significant petroleum discoveries occur in the Beaufort-Mackenzie Basin where anomalously high temperatures are observed. Chen *et al*. (2010a) fit non-linear models to the well temperature data of Hu *et al*. (2010) and observed systematic variations in the shape of temperature-depth profiles. Temperature-depth trends tend to be convex-shaped in the western fold belt and concave-shaped in rapidly deposited Tertiary strata in the eastern and north-central Beaufort Shelf. However, given the uncertainty associated with individual temperature measurements, it is useful to provide a first-order linear fit to the well temperature data. A geothermal gradient map (Issler *et al*., 2011) was

constructed by assuming that deep well temperatures linearly intersect the base of mapped ice-bearing permafrost (IBPF) at 0 °C.

The primary purpose of this report is to document the well temperature data used to prepare the Issler *et al*. (2011) geothermal gradient map and to provide updated geothermal gradient determinations in light of revisions to the base of permafrost interpretations by Hu *et al*. (2013). This report contains temperature-depth plots and tabulated values of quality-assessed geothermal gradient values for the study wells. The quality assessment scheme is based on the quality and number of temperature data points, their spatial distribution, and the quality of the least-squares fit to the data. A revised geothermal gradient map is included in this report.

DATA SOURCES

Subsurface temperature data

Hu *et al.* (2010) developed a quality-assessed borehole temperature dataset for the Beaufort-Mackenzie Basin using fluid temperature data from well testing and log-derived bottomhole temperature (BHT) values recorded on the headers of well logs. For this study, we use a slightly modified version of this dataset that includes 2238 quality-assessed temperature values for 259 wells. Fluid temperature data are from drillstem test (DST) and wireline logging tool (Formation Tester – FT; Formation Interval Tester – FIT; Repeat Formation Tester – RFT; and Modular Formation Dynamics Tester - MDT) measurements. BHT values were measured at or near the bottom of the well by maximum-reading thermometers during logging and were corrected for the cooling effects of mud circulation where possible. Hu *et al*. (2010) give a detailed discussion of measurement errors, temperature corrections, and data quality assessment. Well test temperatures are ranked as either “a” (good – successful test) or “b” (poor – misrun test). BHT values are classified as “a” (excellent), “b” (good), “c” (fair) and “d” (poor), depending on the amount and quality of data available for an equilibrium temperature correction using the Horner plot method.

Figure 1 shows the location of the 259 study wells from which the 2238 quality-assessed temperature values were obtained. There are 1079 BHT values from 259 wells and 1159 fluid test temperature values from 181 wells. A plot of all the borehole temperature values with depth yields an average geothermal gradient of 24.6 °C/km (Fig. 2); data points are identified using different coloured symbols according to their quality ranking and data type (open or solid triangles for BHT values; open or solid circles for well test data). The well test temperature and BHT data exhibit a similar range of values as seen in Figure 3; linear regression gives a geothermal gradient of 25 °C /km (Fig. 3a) for DST data and 24.8 °C/km for the "a", "b", and "c" quality BHT data (Fig. 3b).

Base of ice-bearing permafrost (IBPF)

Hu *et al*. (2013) used multi-parameter geophysical and temperature measurements to define the base of fully frozen ($IBPF_F$) and partially-frozen ($IBPF_P$) ice-bearing permafrost for 265 exploration wells in the Beaufort-Mackenzie Basin. The base of IBPF determinations are ranked as "a" (high reliability), "b" (medium reliability) and "c" (low reliability), depending on the combination of methods used and the quality of data available. In general, the base of $IBPF_F$ is the most reliable pick and this is used as a datum for calculating geothermal gradient values. The "a" or "b" quality repeated shallow temperature survey data indicate that the base of $IBPF_F$ is between -2 °C and 0 °C with most values indicating > -1 °C. For the purpose of geothermal gradient calculation, this boundary is assumed to be uniformly 0 °C across the study area. Minor deviations from this temperature are too small to significantly affect calculated geothermal gradient values. Table 1 lists the depths to the base of $IBPF_F$ that are used for the geothermal gradient calculations.

GEOTHERMAL GRADIENT

Calculation method

The presence of variable thicknesses of relict permafrost (Issler *et al*., 2011; Hu *et al.*, 2013) across the study area indicates that the present mean annual surface temperatures are not a suitable datum for calculating geothermal gradients. Instead, we assume steady-state thermal conditions in which linear geotherms intersect the base of $IBPF_F$ at an assumed temperature of 0 °C. Steady-state thermal conditions are unlikely, given the geologically rapid changes in sea level and surface temperature that controlled permafrost growth and decay during the Quaternary (e.g. Taylor *et al*., 2013), and the rapid Cenozoic deposition rates associated with lower temperatures, suppressed heat flow, and reduced thermal maturity on the Beaufort Shelf (Issler and Snowdon, 1990; Chen *et al*., 2008; Issler *et al*., 2011; Issler *et al*., 2012b). In spite of this, much of the well temperature data can be fit adequately using a linear model.

Geothermal gradient is calculated using equation (1), which describes temperature increasing linearly with depth,

$$T = GZ - Ts \qquad (1)$$

where T is temperature (°C), Z is depth (m) with respect to ground level (GL; onshore) or seafloor (SF; offshore), G is fitted average geothermal gradient (°C/m); Ts is the ground or seafloor temperature intercept (°C); and Ts/G is the depth to base of permafrost (m) at an assumed temperature of 0 °C. The depths of temperature points were corrected to true vertical depths (TVD) for all the wells with directional survey data. Also depths were converted from a kelly bushing (KB) datum to a GL or SF datum by subtracting KB elevation or KB elevation plus water depth for onshore and offshore wells, respectively. For each well temperature data set, a constrained least-squares regression is used to calculate the geothermal gradient by requiring that it intersect the 0 °C isotherm at the base of permafrost. Least-squares calculations are sensitive to data outliers and therefore poor quality data are excluded from the calculations based quality assessment criteria.

Temperature-depth profiles

Standard temperature-depth plots were created for each well data set (e.g., Fig. 4). For each plot, the depth axis ranges from 0 to 5000 m and the temperature axis varies from 0 °C to 160 °C. The depth to base of permafrost is shown in the upper left corner of the plot, and it is labelled according to the method used to define the base and the quality of the determination (see legend below plot for definitions). A, B, C and D represent IBPF determined using temperature surveys, geophysical methods, extrapolated temperature-depth profiles, and other information such as well history reports, respectively; "a" "b" and "c" indicate whether IBPF determinations are of high reliability, medium reliability, or low reliability, respectively. Depth of casing shoe and penetrated stratigraphy (see Fig. 5 for stratigraphic chart) are also shown on the right side of the temperature-depth plot. Based on visual examination of the data, a single linear gradient or a series of linear gradients are established using equation 1 and the constrained linear regression method. In general, only the good quality points are used for the linear regression (usually all the poor well test and poor BHT data are excluded for the calculation). This analysis yields best fit parameters for equation (1) and a corresponding coefficient of determination for assessing how well the data are fit by the linear model (R^2).

Figure 4 shows calculated geothermal gradients for two wells with a good distribution of higher quality temperature data. The Unipkat I-22 well has temperature measurements spanning the range of approximately 800 m to 4300 m within post-rift sediments of the Aklak and Taglu sequences (Fig. 5) and an "a" quality permafrost depth of 86 m from shallow temperature surveys (Fig. 4a). Only the good BHT and DST temperature data were used to calculate a geothermal gradient of 27.7 °C/km with a high coefficient of determination (0.998; Fig. 4a). In Figure 4b, all but one of the temperature data points (one fair BHT point excluded) were used to calculate a geothermal gradient of 29.9 °C/km for the Unak L-28 well. The high coefficient of determination (0.981) suggests that the linear model provides a reasonable fit to the data. This well is located near the southern basin margin and penetrated prerift (Permian and older), synrift (Jurassic-Lower Cretaceous) and postrift (Upper Cretaceous-Tertiary) strata (Fig. 5).

In some cases, temperature data from successful DSTs are obviously anomalous and must be excluded from the calculation of average geothermal gradient. For example, in Figure 6a, there is a cluster of anomalously low DST temperature values over the interval, 1770 to 1911 m, for the Ya Ya P-53 well where < 100 m of gas cut mud were recovered during testing. The low temperatures may be related to the Joule-Thomson effect where the pressure drop accompanying flow leads to the expansion and cooling of gases (e.g., Steffensen and Smith, 1973; App, 2008, 2009), resulting in an apparent dogleg geothermal gradient. Only the good DST temperatures (excluding circled anomalous points) were used to calculate an average geothermal gradient of 35 °C/km for the Ya Ya P-53 well (Fig. 6a).

The opposite situation occurs for the Unark L-24 and Unark L-24A wells where the deepest DST temperatures (circled points) are higher than an uncorrected BHT value at a similar depth by about 6.1~10.5°C. Although the temperature data are variable, the deeper DST values appear to be offset with respect to the linear trend line for the better quality data (red dashed line in Fig. 6b). Shale sonic porosity, mud weight and DST fluid pressure data indicate that the higher DST temperatures are from an overpressured zone with shut-in pressure values up to 74.3 MPa (Fig. 6b). Gas, oil and water were recovered from this zone. The higher DST temperatures may be the result of Joule-Thomson expansion which can increase the temperature of oil and gas reservoir fluids under high drawdown pressures (App, 2008, 2009). The excellent and good BHT data, and the good DST temperature data (excluding circled anomalous points) yield an average geothermal gradient of 25.7 °C/km (Fig. 6b).

For the Parsons P-53 well there is an apparent sharp increase in temperature below 3000 m (Fig. 7a). The high DST temperatures (circled points) are assumed to be anomalous and were excluded from the geothermal gradient calculation. Mixed fluids (610 m of water cushion, 181 m of muddy water, 713 m of mud, and 296 m of salt water) were recovered at this depth. The reason for the high temperatures is unclear. Although the Joule-Thomson effect can result in warming of liquids, the effect is generally small for typical pressure drops. App (2008) calculated that pressure drawdowns between 13.8 MPa to 68.9 MPa (2000 – 10000 psia) can result in temperature increases of 2 °C to 13 °C which is less than the apparent temperature increase in the Parsons P-53 well (17 °C

to 31 °C with respect to trend line temperature of 90 °C at 3345 m). It is unlikely that pressure drawdowns would exceed this range for the Parsons P-53 well.

The Parsons F-09 well also exhibits anomalously high DST temperatures (118 °C at nearly 3000 m; Fig. 7b). The shallower DST encountered gas with a gas to surface flow rate of 487,000 m^3/d whereas the deeper DST recovered mixed fluids (mud, muddy water and salt water). A nearby excellent quality corrected BHT measurement (89 °C at 3105 m) has a much lower temperature than the DSTs and it yields an average geothermal gradient of 32 °C/km which is similar to other Parsons wells. Therefore, the DST temperatures are considered erroneously high but the reasons for this are unknown.

Some apparently fair to good quality BHT and DST temperature values appear to be anomalously high at shallow depth with respect to the base of IBPF and deeper temperature trends (Fig. 8). Majorowicz *et al*. (1990) first noted that many BHT values at < 1.5 km depth were too high and inconsistent with calculated geotherms that matched deeper data and temperature at the base of permafrost. Therefore, they questioned the reliability of shallow BHT data. There are more shallow BHT data (Fig. 3b) than shallow DST temperature data (Fig. 3a) and the effect of the anomalous BHT data is to shift the surface temperature intercept to more positive values on the temperature depth plot (surface intercept is 1.8 °C in Fig. 3b versus -0.3 °C in Fig. 3a).

In Figure 8a, high shallow DST temperature may indicate that fluids were recovered from the thermally disturbed zone around the borehole rather from pristine formation fluids beyond from the invaded zone. The anomalous DST temperature was not used for calculating a geothermal gradient of 34.1 °C/km for the Atigi G-04 well. In some Beaufort-Mackenzie wells, multiple BHT values at shallow depth show a decline in temperature with time which indicates that the formation was heated by warmer drilling fluids (Figure 8b), the shallow BHT value was not used to calculate the average geothermal gradient of 27.8 °C/km for the Amerk O-09 well.

Some authors have reported a “dogleg” type of increase in geothermal gradient below the top of overpressured zones in some basins (e.g. Jones, 1969; Law *et al*., 1998; Nashaat, 1998). An increase in geothermal gradient could be caused by changes in rock thermal properties that are related to changes in lithology, porosity and/or rock texture. For the Beaufort-Mackenzie Basin, the main zone of overpressure is associated with

thick, undercompacted Cenozoic strata and it can be defined using well logs, DST and mud weight data (Issler, 1992; Issler *et al*., 2002; Chen *et al*., 2010b; Issler *et al*., 2011). The diagnostic log signatures of overpressured zones may be compatible with physical property changes that could increase the geothermal gradient but there is no clear evidence for this in the Beaufort-Mackenzie Basin. Some Beaufort-Mackenzie wells can be interpreted as having a dogleg increase in temperature through the overpressured zone (Fig. 6b) but the uneven and sparse distribution of data and the associated measurement errors can make it difficult to justify more than a first-order fit to the data. Also, as shown in Figure 7, measurement errors can lead to apparent dogleg geothermal gradients. Although elevated geotherms within overpressured zones are difficult to document, some apparent thermal anomalies in the basin may be related to upward flow of fluids along faults driven by high fluid pressure gradients (e.g. Chen *et al*., 2008; Issler *et al*., 2011).

Figure 9 shows variable temperature data within the overpressured zone of the Mallik A-06 well. Shale sonic transit-time and sonic porosity trends indicate that the top of the main overpressured zone occurs at 3070 m (Fig. 9a). Above this depth, sediments appear to be normally compacted but DST and mud weight data indicate a second zone of overpressure extending up to approximately 2340 m (Fig. 9b). The origin of this shallower zone of overpressure is unclear but it may be related to post-compaction pressure-charging. Anomalously low DST temperature values (circled values) within the overpressured zone of the Mallik A-06 well may be the result of the Joule-Thomson effect associated with flowing gas as described above (Fig. 9c). Gas is strongly implicated by the presence of Upper Cretaceous-derived (Smoking Hills/Boundary Creek formations) biodegraded oil (Issler *et al*., 2012a) and high alkalinity fluid (Grasby *et al*., 2009) within overpressured sediments of the Richards and Taglu sequences. Grasby *et al*. (2009) suggest that the high alkalinity fluid formed by anaerobic methanogenesis under a closed system due to rapid burial and overpressure development. Further evidence for gas includes well log indicators for a gas zone and the recovery of gas cut mud recorded for a DST (Fig. 9c). The dashed red lines could indicate an elevated geothermal gradient in the overpressured zone (35.5 °C/km versus 30 °C/km for the overlying section). However, given the limitations of the data, we prefer the average geothermal gradient determined using the better quality data (31.5 °C/km; Fig. 9c).

Figure 10 shows another example of a well with overpressure and variable temperature data. The top of overpressure is well defined for the Kumak J-06 well at approximately 2400 m based on DST pressure data (Fig. 10b) and log data (Fig. 10a). Mud pressure data indicate that the well was drilled overbalanced with respect to formation pressure (as measured by DSTs) from approximately 700 m to 2400 m. Near 700 m depth, a DST recovered gas with a flow rate of 33,000 m^3/d (red area; Fig. 10c) which suggests that mud density was increased to control potential gas kicks. The blue area indicates where DSTs recovered mixed fluids and sand. Temperature data in the upper 1700 m are generally of good quality and conform to a linear trend (red dashed line). Below 1700 m, poor quality BHTs and DST temperatures are anomalously low. The low DST values can be explained by the Joule-Thomson effect associated with flowing gas. The purple area highlights DSTs with a total flow rate of 283,000 m^3/d of oil and gas (Fig. 10c). In contrast, the shallow gas zone shows little if any Joule-Thomson effect, probably due to the much smaller pressure drop associated with gas flow. A single excellent quality BHT value near 2400 m was included with the temperature data above 1700 m to calculate an average geothermal gradient of 32.2 °C/km (Fig. 10c).

Geothermal gradient quality assessment

Geothermal gradient is calculated from the well temperature data and a constrained permafrost base with an assumed temperature of 0 °C. Quality levels are assigned to calculated geothermal gradients based on: 1) the number and quality rank of temperature data points used for the regression calculation; 2) the quality of the least squares linear regression fit to the data as assessed by the coefficient of determination (R^2); and (3) the distribution of data with respect to the regression line. The criteria for quality ranking of geothermal gradient values are summarized below:

a- Excellent (more than three temperature data points with good coverage in depth) Excellent or good BHT values (“a” or “b” quality) plus temperature values from successful well test data and all the data show a high coefficient of determination ($R^2 > 0.9$) with minimal scatter around the linear regression line (Fig. 4).

b- Good (one of two cases; data show fair coverage in depth)

(1) three or more data points from excellent/good BHT data ("a" or "b" quality) and/or good DST data but the data are more scattered or there is less consistency between corrected BHTs and DST temperatures ($R^2 > 0.9$);

(2) two or more good well test/excellent and/or good BHT values and consistent BHT or poor DST values displaying good coverage with depth ($R^2 > 0.9$).

c- Fair (one of four cases)

(1) two excellent/good BHT or good well test values ($R^2 > 0.8$);

(2) at least one good well test/excellent BHT/good BHT value and one or more fair BHT or poor DST data points that show good consistency ($R^2 > 0.8$);

(3) at least one good well test/excellent BHT/good BHT value and two or more poor BHT or poor DST data points that show good consistency ($R^2 > 0.8$);

(4) three or more fair BHT values ($R^2 > 0.8$).

d- Poor (one of four cases)

(1) multiple fair BHT values but with poor coverage in depth;

(2) fewer than three fair BHT values plus poor BHT and/or poor well test values;

(3) only poor BHT/DST data;

(4) R^2 value cannot be calculated.

Figures 4, 8, 11 and 12 illustrate calculated geothermal gradient values with quality rankings of "a", "b", "c", and "d", respectively. Calculated geothermal gradients range in quality from "a" to "c" for approximately 77% of the 259 study wells; about 56% of the wells have geothermal gradients of "a" or "b" quality (Table 1).

Geothermal gradient distribution

Average geothermal gradients were derived from quality ranked BHT (corrected for drilling mud circulation) and well test temperature data for 259 wells (Table 1). Detailed plots of temperature versus depth and calculated geothermal gradient for the study wells are shown in alphabetic order by well name in Appendix A (Aagnerk E-56 to Ivik N-17 wells; Figs. 13 to 79), Appendix B (Kadluk O-07 to Minuk I-53 wells; Figs. 80 to 128),

Appendix C (N. Ellice J-23 to Spring River YT N-58 wells; Figs. 129 to 197), and Appendix D (Taglu C-42 to Ya Ya P-53 wells; Figs. 198 to 255).

Calculated geothermal gradients vary between approximately 15 °C/km to 48 °C/km (Table 1). Figure 256 shows that most (78 %; > 200 wells) of the calculated geothermal gradients for the Beaufort-Mackenzie Basin have typical sedimentary basin values that range from 25 °C/km to 35 °C/km; >39% are between 25 °C/km to 30 °C/km and approximately 39% are between 30 °C/km to 35 °C/km. Given the uneven distribution of wells across the study area, the geothermal gradient map has been hand-contoured using a relatively coarse contour interval (5 °C/km) to show a relationship between geothermal gradient and structural trends (Fig. 257; modified from Issler *et al*., 2011). The southeast margin of the basin is marked by higher geothermal gradients (from approximately 30 °C/km to 50 °C/km). As discussed by Issler *et al*. (2011), this region of relatively intact continental crust is marked by Jurassic-Early Cretaceous extension faults of the Eskimo Lakes Fault zone; higher gradients may be associated with higher radiogenic heat production and fault-related fluid flow. In contrast, temperature gradients in the fold belt on the southwest margin of the basin are markedly lower but there is very limited well control to constrain contouring. In the far offshore region encompassing the Kenalooak J-94 well, geothermal gradients are low (< 25 °C/km), probably as the result of heat flow suppression by rapid burial of the Plio-Pleistocene Iperk Sequence. The central portion of the basin is warmer with geothermal gradients >30 °C/km and part of this region coincides with the Tarsiut-Amauligak Fault Zone.

DISCUSSION

This report presents the results of a simple but useful analysis of the quality-assessed well temperature data compiled by Hu *et al*. (2010) for the Beaufort-Mackenzie Basin. By visually displaying temperature data versus depth, anomalous temperature values are recognized easily and can be eliminated from the calculation of average geothermal gradient. Anomalous temperature values are not confined to the lower quality BHT (quality "c" and "d") and DST (quality "b" – misrun) data as defined by Hu *et al*. (2010) but they may include some apparently higher quality values as well. Hu *et al*. (2010)

provide a detailed discussion of various sources of error for BHT and DST measurements.

Generally, the poorer quality data (e.g., uncorrected BHTs, misrun DSTs) tend to underestimate true formation temperatures, especially in the deeper parts of wells, due to drilling related factors (e.g., formation invasion and cooling by circulating drilling mud) and these data will lead to underestimates of geothermal gradient if included in the analysis. Even successful "a" quality DSTs with high flow rates can yield anomalously low temperatures (Figs. 6a, 9c, and 10c), and some DST temperatures are higher at high pressures (Fig. 6c) probably due to the Joule-Thomson effect for gas and oil reservoirs (App, 2008, 2009). These DST values were excluded from geothermal gradient calculations when information was available to constrain DST interpretations. Anomalously high temperatures have been observed beneath the permafrost at shallow depths (upper 1000 m or so) in this study and by previous workers (Majorowicz *et al*., 1990). It appears that warm drilling muds have heated up formations around the borehole and this has affected DST but especially BHT measurements (Fig. 3).

Unlike the shallow temperature measurements, it is more difficult to account for anomalously high deep temperature values (e.g., Fig. 7a and 7b). Available measurement techniques are applied under less than ideal conditions and tend to variably underestimate true *in situ* formation temperatures in response to various borehole environmental factors. However, the Joule-Thomson and transient fluid expansion/compression effects can lead to decreases or increases in temperature. In the case of high drawdown completions, the Joule-Thomson effect can lead to DST temperatures that are somewhat higher than *in situ* reservoir fluid temperatures (generally < 10 °C) (App, 2008 and 2009). This process cannot account for the 30 °C to 40 °C shift in temperature that is observed for some wells. Such implied steep increases in temperature gradient, if attributed to natural processes, imply heat advection by fluid flow or transient heating by geologically recent emplacement of a nearby heat source. Alternatively such values are erroneous and must be rejected, whether they are the result of inaccurate recording of temperature data, incorrect instrument calibration, or physical interference with the measurement device (there have been anecdotal stories of hot steam being used to clean mud off measuring instruments for some northern wells). Oxburgh and Wilson (1989) mention that

anomalously high BHT values can be caused by boiling water that has been trapped accidentally within maximum-recording mercury-in-glass thermometers.

In general, only the higher quality BHT and DST data were used to calculate geothermal gradient. In some cases, fair ("c" quality) BHT data were used for wells having limited temperature data and most of these fair quality BHT data are consistent with the higher quality data. Sometimes poor quality values were used for wells with sparse temperature data even though true temperatures may be underestimated. Quality assessment gives an indication of the reliability of geothermal gradient values based on the nature of the data used for the calculations.

Some of the geothermal gradient values used by Issler *et al*. (2011) have been revised (Table 1) based on a re-evaluation of the well temperature data used for the calculations (e.g., Fig. 10) and the use of an updated permafrost datum (Hu *et al*., 2013) for the constrained regression analysis. The updated geothermal gradient map (Fig. 257) is generated using 253 of 259 calculated geothermal gradients; six average gradient values with "d" quality ranking are excluded in the contour mapping because they are obviously low (e.g., Onigat C-38 well, Fig.159 in Appendix C) or questionable (e.g., Aklavik F-17 well, Fig. 24 in Appendix A). However, the new interpreted contour map (Fig. 257) is similar to the map of Issler *et al*. (2011) in defining the main areas of high and low geothermal gradient; there are differences in the shape of some contours and in the presence or absence of small thermal anomalies. These results are extremely important for basin thermal history studies because temperature is a key parameter for calibrating basin thermal models.

CONCLUSIONS

Average geothermal gradients were determined for 259 Beaufort-Mackenzie wells by linear least-squares fitting of quality-selected deep well temperature data. Gradients were constrained to intersect 0 °C at the mapped base of permafrost for each well and only the higher quality temperature data were used for the calculations when possible. Excluded anomalous low temperature values include lower quality data from DST and BHT measurements, and DST measurements from gas intervals (cooling related to Joule-

Thomson effect). Excluded anomalous high temperature values include shallow DST and BHT measurements from beneath the permafrost in wells believed to have experienced drilling-induced heating, DST measurements from oil and gas zones (heating related to Joule-Thomson effect), and discordant extreme DST and BHT values (up to 30 °C to 40 °C higher than background values) at greater depths. Geothermal gradient values were quality-ranked based on the nature of the data used for the calculations and the quality of the fit to the data. Approximately 56% of geothermal gradient determinations are of "a" (excellent) or "b" (good) quality whereas 77% of the well gradients range from "a" to "c" (fair) quality.

Geothermal gradients vary between 15 °C/km and 48 °C/km with > 200 wells (78%) having values between 25 °C/km and 35 °C/km. An updated, hand-contoured geothermal gradient map shows that high gradients (> 30 °C/km) are associated with Jurassic-Lower Cretaceous rift faults and intact continental crust of the southeast basin margin (Tuktoyaktuk Peninsula), and major onshore and offshore Tertiary faults of the Tarsiut-Amauligak and Taglu fault zones. Very low gradients (<25 °C/km) occur in rapidly deposited Plio-Pleistocene strata on the outer Beaufort shelf. Elsewhere, much of the basin is characterized by typical sedimentary basin geothermal gradients of 25 °C/km to 30 °C/km.

ACKNOWLEDGEMENTS

We thank Dr. Gilles Bellefleur of the GSC Central Canada Division for his careful review of this report, professor Gary Gang Zhao (University of Regina) for his valuable discussions concerning well testing, Tom Brent for help with preparing the basemap for the well location, and Christine Deblonde for assistance in update of geothermal gradient contour map. This study would not have been possible without access to the publicly available well history reports curated by the National Energy Board (NEB) of Canada. Funding was provided by the former Beaufort-Mackenzie consortium of companies (Anadarko Canada Corporation, BP Canada Energy Company, Chevron Canada Limited, ConocoPhillips Canada Resources Corporation, Devon Canada Corporation, EnCana Corporation, Imperial Oil Resources Ventures Limited, MGM Energy Corporation, Petro-Canada (now Suncor), Shell Canada Limited, and Shell Exploration and Production Company), the Program of Energy Research and Development (PERD), and Natural Resources Canada through the Earth Sciences Sector Northern Resources Development (2003-2006), Secure Canadian Energy Supply (2006-2009), and Geo-Mapping for Energy and Minerals (GEM) (2009-2013) programs. This work was completed under the GEM Mackenzie Delta and Corridor project led by Dr. Robert MacNaughton of GSC Calgary and we thank him for his support and encouragement.

REFERENCES

App, J.F., 2008. Nonisothermal and productivity behaviour of high pressure reservoirs. SPE 114705 presented at the 2008 SPE Annual Technical Conference and Exhibition, Denver, Colorado, September 21-24, 19 p.

App, J.F., 2009. Field cases: Nonisothermal behavior due to Joule - Thomson and transient fluid expansion/compression effects. Paper SPE 124338 presented at the SPE Annual Technical Conference and Exhibition, New Orleans, Louisiana, USA, October 4-7, 13 p.

Bachu, S. and Burwash, R.A., 1994. Geothermal Regime in the Western Canadian Sedimentary Basin. *In*: Geological Atlas of the Western Canada Sedimentary Basin. G. D. Mossop and I. Shetsen (eds.). Canadian Society of Petroleum Geologists and Alberta Research Council, p. 447-454.

Barker, C., 1996. Thermal Modelling of Petroleum Generation: Theory and Applications. Developments in Petroleum Science, 45, Elsevier, Amsterdam, The Netherlands, 512 p.

Chen, Z., Osadetz, K.G., Issler, D. R., and Grasby, S. E., 2008. Hydrocarbon migration detected by regional temperature field variations, Beaufort-Mackenzie Basin, Canada. American Association of Petroleum Geologists Bulletin, v. 92, no. 12, p. 1639-1653.

Chen, Z., Issler, D. R., and Hu, K., 2010a. A non-linear fit to formation temperature profiles from petroleum exploration wells in the Beaufort-Mackenzie Basin, Canada. Geological Survey of Canada, Open File 6216, 16 p. doi: 10.4095/262721

Chen, Z., Osadetz, K.G., Issler, D.R., and Grasby, S.E., 2010b. Pore pressure patterns in Tertiary successions and hydrodynamic implications, Beaufort-Mackenzie Basin, Canada. Bulletin of Canadian Petroleum Geology, v. 58, no. 1, p. 3-16.

Dixon, J., Morrow, D.W., and MacLean, B.C. 2007. A Guide to the Hydrocarbon Potential of the Northern Mainland of Canada. Geological Survey of Canada, Open File 5641, 46 p. doi:10.4095/224377.

Grasby, S.E., Chen, Z., Issler, D., and Stasiuk, L., 2009. Evidence for deep anaerobic biodegradation associated with rapid sedimentation and burial in the Beaufort-Mackenzie basin, Canada. Applied Geochemistry, v. 24, p. 536-542.

Grasby, S.E., Allen, D.M., Bell, S., Chen, Z., Ferguson, G., Jessop, A., Kelman, M., Ko, M., Majorowicz, J., Moore, M., Raymond, J., and Therrien, R., 2012. Geothermal Energy Resource Potential of Canada. Geological Survey of Canada, Open File 6914 (revised), 322 p. doi:10.4095/291488

Hu, K., Issler, D.R., and Jessop, A., 2010. Well temperature data compilation, correction and quality assessment for the Beaufort-Mackenzie Basin. Geological Survey of Canada, Open File 6057, 17 p. doi:4095/262755

Hu, K., Issler, D.R., Chen, Z., and Brent, T.A., 2013. Permafrost investigation by well logs, and seismic velocity and repeated shallow temperature surveys, Beaufort-Mackenzie Basin. Geological Survey of Canada, Open File 6956, 33 p. doi:4095/293120

Issler, D.R., 1984. Calculation of organic maturation levels for offshore eastern Canada - implications for general application of Lopatin's method. Canadian Journal of Earth Sciences, v. 21, p. 474-488.

Issler, D.R., 1992. A new approach to shale compaction and stratigraphic restoration, Beaufort-Mackenzie Basin and Mackenzie Corridor, northern Canada. American Association of Petroleum Geologists Bulletin, v. 76, p. 1170-1189.

Issler, D.R. and Snowdon, L.R., 1990. Hydrocarbon generation kinetics and thermal modelling, Beaufort-Mackenzie Basin. Bulletin of Canadian Petroleum Geology, v. 38, p. 1-16.

Issler, D.R., Katsube, T.J., Bloch, J.D., and McNeil, D.H., 2002. Shale compaction and overpressure in the Beaufort-Mackenzie Basin of northern Canada. Geological Survey of Canada, Open File 4192, 10 p. (1 diskette) doi:10.4095/213052

Issler, D.R., Hu, K., Lane, L.S. and Dietrich, J.R., 2011. GIS compilations of overpressure, permafrost distribution, geothermal gradient and geology, Beaufort-Mackenzie region, Northern Canada. Geological Survey of Canada, Open File 5689 (1 CD-ROM), doi:10.4095/289113.

Issler, D.R., Obermajer, M., Reyes, J., and Li, M., 2012a. Integrated analysis of vitrinite reflectance, Rock-Eval 6, gas chromatography, and gas chromatography-mass spectrometry data for the Mallik A-06, Parsons N-10 and Kugaluk N-02 wells, Beaufort-Mackenzie Basin, northern Canada. Geological Survey of Canada, Open File 6978, 78 p. doi: 10.4095/289672

Issler, D.R., Reyes, J., Chen, Z., Hu, K., Negulic, E., Grist, A., Stasiuk, L., and Goodarzi, F., 2012b. Thermal History Analysis of the Beaufort-Mackenzie Basin, Arctic Canada. *In*: Papers Presented at the 32nd Annual Gulf Coast Section, Society of Economic Paleontologists and Mineralogists Foundation Bob F. Perkins Research Conference, v. 32, p. 609-641. (DVD)

Jones, P.H., 1969. Hydrodynamics of Geopressure in the Northern Gulf of Mexico Basin. Journal of Petroleum Technology, v. 21, p. 803-810.

Jones, F.W., Majorowicz, J.A., and Dietrich, J., 1988. The geothermal regime of the northern Yukon and Mackenzie Delta regions of northern Canada – studies of two regional profiles. Pure and Applied Geophysics, v. 127, no. 4, p. 641-658.

Jones, F.W., Majorowicz, J.A., Dietrich, J., and Jessop, A.M., 1990. Geothermal gradients and heat flow in the Beaufort-Mackenzie Basin, arctic Canada. Pure and Applied Geophysics, v. 134, no. 3, p. 473-483.

Law, B.E., Shah, S.H.A., and Malik, M.A., 1998. Abnormally high formation pressures, Potwar Plateau, Pakistan. *In*: Abnormal pressures in hydrocarbon environments. B.E. Law, G.F. Ulmishek and V.I. Slavin (eds). American Association of Petroleum Geologists, Memoir 70, p. 247-258.

Majorowicz, J.A., Jones, F.W. and Jessop, A.M., 1988. Preliminary geothermics of the sedimentary basins in the Yukon and Northwest Territories (60°N - 70°N) – estimates from petroleum bottom-hole temperature data. Bulletin of Canadian Petroleum Geology, v. 36, no. 1, p. 39-51.

Majorowicz, J.A., Jones, F.W., and Judge, A.S., 1990. Deep subpermafrost thermal regime in the Mackenzie Delta basin, northern Canada – analysis from petroleum bottom-hole temperature data. Geophysics, v. 55, no. 3, p. 362-371.

Majorowicz, J.A., Jessop, A.M., and Judge, A.S., 1996. Geothermal Regime. *In*: Geological Atlas of the Beaufort-Mackenzie Area. J. Dixon (ed.). Geological Survey of Canada, Miscellaneous Report 59, p. 33-37.

Majorowicz, J.A. and Embry, A.F., 1998. Present heat flow and paleo-geothermal regime in the Canadian arctic margin: analysis of industrial thermal data and coalification gradients. Tectonophysics, v. 291, p. 141-159.

Majorowicz, J.A. and Morrow, D.W., 1998. Subsurface temperature and heat flow – Yukon and Northwest Territories. Geological Survey of Canada, Open File 3626, 29 p. doi:10.4095/209923

Majorowicz, J.A., Jessop, A.M., and Lane, L.S., 2005. Regional heat flow pattern and lithospheric geotherms in northeastern British Columbia and adjacent Northwest Territories, Canada. Bulletin of Canadian Petroleum Geology, v. 53, no. 1, p. 51-66.

Moir, P.N. and Bell, J.S., 1989. Geochemistry I, Labrador Sea, Geothermal Gradients and Depth to Gas Generation. *In*: Labrador Sea. J.S. Bell, R.D. Howie, N.J. McMillan, C.M. Hawkins and J.L. Bates (eds.). Geological Survey of Canada, East Coast Basin Atlas Series, p. 86-87. doi:10.4095/127196

Nashaat, M., 1998. Abnormally high fluid pressure and seal impacts on hydrocarbon accumulations in the Nile Delta and North Sinai Basins. *In*: Abnormal pressures in hydrocarbon environments. B.E. Law, G.F. Ulmishek and V.I. Slavin (eds). American Association of Petroleum Geologists, Memoir 70, p. 161-180.

Oxburgh, E.R. and Wilson, N., 1989. Temperature, fluid flow, and hydrocarbon maturation. *In*: Handbook of Seafloor Heat Flow. J.A. Wright and K.E. Louden (eds.). CRC Press Inc., Boca Raton, Florida, p. 191-229.

Steffensen, R.J. and Smith, R.C., 1973. The importance of Joule-Thomson heating (or cooling) in temperature log interpretation. SPE 4636 presented at the 48th Annual Fall Meeting of the Society of Petroleum Engineers of AIME, Las Vegas, September 30-October 3.

Taylor, A.E., Dallimore, S.R., Hill, P.R., Issler, D.R., Blasco, S., and Wright, F., 2013. Numerical model of the geothermal regime on the Beaufort Shelf, arctic Canada since the Last Interglacial. Journal of Geophysical Research: Earth Surface, v. 118, p. 2365-2379, doi:10.1002/2013JF002859

LIST OF TABLES

LIST OF FIGURES